IOPscience iopscience.iop.org

Home Search Collections Journals About Contact us My IOPscience

Electron-beam and ion-beam-induced deposited tungsten contacts for carbon nanofiber interconnects

This content has been downloaded from IOPscience. Please scroll down to see the full text.

2014 Nanotechnology 25 375702

(http://iopscience.iop.org/0957-4484/25/37/375702)

View the table of contents for this issue, or go to the journal homepage for more

Download details:

IP Address: 152.135.235.188
This content was downloaded on 25/08/2014 at 17:03

Please note that terms and conditions apply.

IOP Publishing | Nanotechnology

Nanotechnology 25 (2014) 375702 (8pp) doi:10.1088/0957-4484/25/37/375702

Electron-beam and ion-beam-induced deposited tungsten contacts for carbon nanofiber interconnects

Patrick Wilhite[1], Hyung Soo Uh[2], Nobuhiko Kanzaki[1], Phillip Wang[3], Anshul Vyas[1], Shusaku Maeda[4], Toshishige Yamada[1,5] and Cary Y Yang[1,6]

[1] Center for Nanostructures, Santa Clara University, Santa Clara, CA 95053, USA
[2] Electronics Engineering, Sejong University, Seoul, Korea
[3] Applied Materials, Santa Clara, CA 95052, USA
[4] Hitachi High-Technologies Corporation, Ibaraki, Japan
[5] Electrical Engineering, University of California Santa Cruz, Santa Cruz, CA 95064, USA

E-mail: cyang@scu.edu

Received 23 April 2014, revised 7 July 2014
Accepted for publication 17 July 2014
Published 22 August 2014

Abstract

Ion-beam-induced deposition (IBID) and electron-beam-induced deposition (EBID) with tungsten (W) are evaluated for engineering electrical contacts with carbon nanofibers (CNFs). While a different tungsten-containing precursor gas is utilized for each technique, the resulting tungsten deposits result in significant contact resistance reduction. The performance of CNF devices with W contacts is examined and conduction across these contacts is analyzed. IBID-W, while yielding lower contact resistance than EBID-W, can be problematic in the presence of on-chip semiconducting devices, whereas EBID-W provides substantial contact resistance reduction that can be further improved by current stressing. Significant differences between IBID-W and EBID-W are observed at the electrode contact interfaces using high-resolution transmission electron microscopy. These differences are consistent with the observed electrical behaviors of their respective test devices.

Keywords: metal–carbon nanotube contact, contact resistance, electron beam induced deposition, ion-beam-induced deposition

(Some figures may appear in colour only in the online journal)

1. Introduction

Metallization techniques are frequently used during post-fabrication contact engineering for carbon-based nanomaterials to mitigate the high contact resistances between these materials and their contact electrodes. Metal depositions induced by ionic currents, such as electron-beam-induced deposition (EBID) and ion-beam-induced deposition (IBID), offer point-and-shoot capability which can lead to contact improvement. EBID of metals has been reported since the 1960s, and has received much attention in recent years [1–8] for various applications such as etching and deposition [3], as well as fabricating nanowires [4], field emission tips [7], and atomic force microscope probes [8]. A major drawback of EBID deposits is the high impurity levels originating from either incomplete decomposition of the precursor gas, or residual impurities within the deposition chamber. Because of this sensitivity to impurities, EBID deposits are subjected to careful deposition parameter controls, and it is not uncommon for the deposits to undergo additional purification steps [9]. IBID deposits, on the other hand, result in significantly higher purities. Focused ion beam (FIB) using gallium (Ga) ions is capable of inducing metal depositions by delivering high energy to dissociate the precursor, along with possible localized heating at the impingement surface. However, this high-energy Ga ion beam could have deleterious effects as it can

[6] Author to whom any correspondence should be addressed.

 © 2014 IOP Publishing Ltd Printed in the UK

create defects in the substrate and unintended Ga ion implantation that can potentially alter the electrical properties of junctions and transistors [10]. In recent years, various metals have been used in IBID and EBID experiments to improve contacts [11–14]. In particular, tungsten (W) contacts formed by IBID or EBID have proven to be effective in reducing contact resistance in carbon nanofiber (CNF) interconnects [14, 15].

Carbon-based nanostructures such as carbon nanotubes (CNTs) [17–19] and CNFs [20–22] are candidate materials for next-generation semiconductor devices and integrated circuits (IC) due to their tolerance to electromigration under high currents and excellent electrical, thermal, and mechanical properties [23–27]. Understanding the physical origin of CNF/metal contact resistance, and minimizing it are essential for functionalizing these materials in applications where high electrical conduction is critical.

Many as-fabricated test devices consisting of a CNF bridging two electrodes result in very high resistances typically in the MΩ range, as well as nonlinear current–voltage (*I–V*) characteristics due to the formation of tunneling barriers [28]. Such non-ohmic behavior has been observed for CNF vias and interconnects [22, 29, 30]. Generally, contact resistance can be improved by current stressing and/or contact metallization. In particular, current stressing results in linear *I–V* behavior and reduction in contact resistance to a few tens of kΩ or less. Nevertheless, such improvements are not sufficient in terms of contact resistance reduction and consistency.

The use of EBID-W or IBID-W as a contact engineering technique avoids the need for extra masking steps required in other metal deposition schemes, making them versatile tools for nanocarbon device fabrication. And tungsten deposits with EBID and IBID, respectively, provide a common metal to evaluate and compare these two techniques. In this paper, the use of EBID and IBID to fabricate W contacts is investigated as means to improve the contact resistance between CNF and gold (Au) electrodes. Compared with other metals based on the their interface properties, Au and W are not necessarily the best candidates for making electrical contacts to carbon nanostructures [31, 32]. However, suitable contact engineering between CNF and these metals is shown to lead to relatively low contact resistance. Further, comparisons are made of the interfacial nanostructures at the electrode contacts using transmission electron microscopy (TEM) and energy dispersive x-ray spectroscopy (EDS), which are correlated with analysis of conduction across these contacts based on current stressing measurements and a simple circuit model.

2. Sample preparation and electrical measurements

Test devices are prepared by drop-casting a single CNF between a pair of Au electrodes patterned on a silicon dioxide (SiO_2) substrate [22]. IBID-W contacts are then formed using FIB deposition [16]. After the depositions, the resulting total device resistances generally decrease by a factor of 10–100. Our results are consistent with reported improvement of contact resistance due to metal deposition on electrode contacts in nanoscale devices [15, 16] and suitable for many potential applications in IC technology where W is frequently used. On the other hand, EBID provides finer control for metal depositions in the nanoscale with little damage to the substrate. Our experiments show that both IBID-W and EBID-W are effective in reducing contact resistance in CNF test devices.

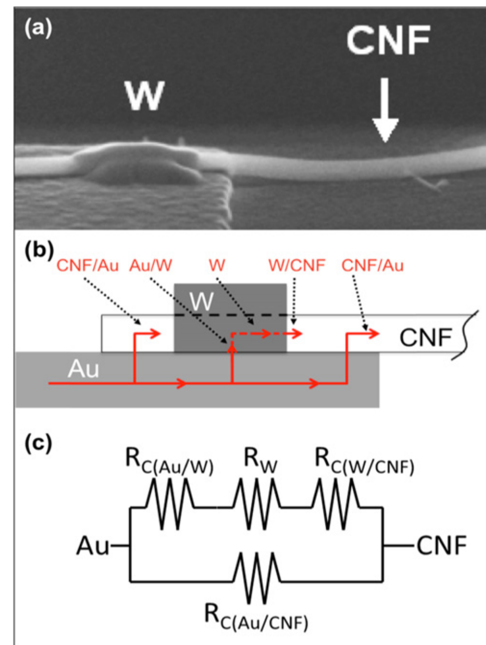

Figure 1. (a) SEM images of CNF test devices, (b) schematic representation of current paths through various interfaces and W deposit at the CNF/Au/W contact, and (c) corresponding equivalent circuit.

For EBID, the precursor gas is delivered via a gas injection system (GIS) [33] in the chamber of a scanning electron microscope (SEM). The chamber is plasma-cleaned to the extent that no carbon deposits are detected after e-beam irradiations in excess of 30 min. With a slow raster scan rate leading to higher beam dwell times, higher purity deposits are expected as previously reported [9]. The e-beam acceleration voltage is 30 kV, with an emission current of 100–150 μA (resulting in substrate currents of 65–100 pA) and a working distance of 11–12 mm. WF_6 is delivered to the surface of the sample via the GIS, and the e-beam facilitates the dissociation of WF_6, yielding W deposit in the area where it impinges upon the substrate. The amount of deposit depends on the e-beam scanning time. The total raster time at the target area during e-beam impingement is 15–20 min per contact pad. A similar GIS system is used for IBID with a FIB system and $W(CO)_6$ as the W source. In this case, acceleration voltage is also 30 kV with a working distance of 5.6 mm, while the deposition time is 24 s per contact pad. The vacuum pressures are 1.5×10^{-3} Pa and 9.0×10^{-5} Pa in the SEM and FIB chambers, respectively.

Deposition sizes and rates for W are adjusted such that the deposits will not spread laterally over the target area. For our configuration, the optimized deposition sizes are

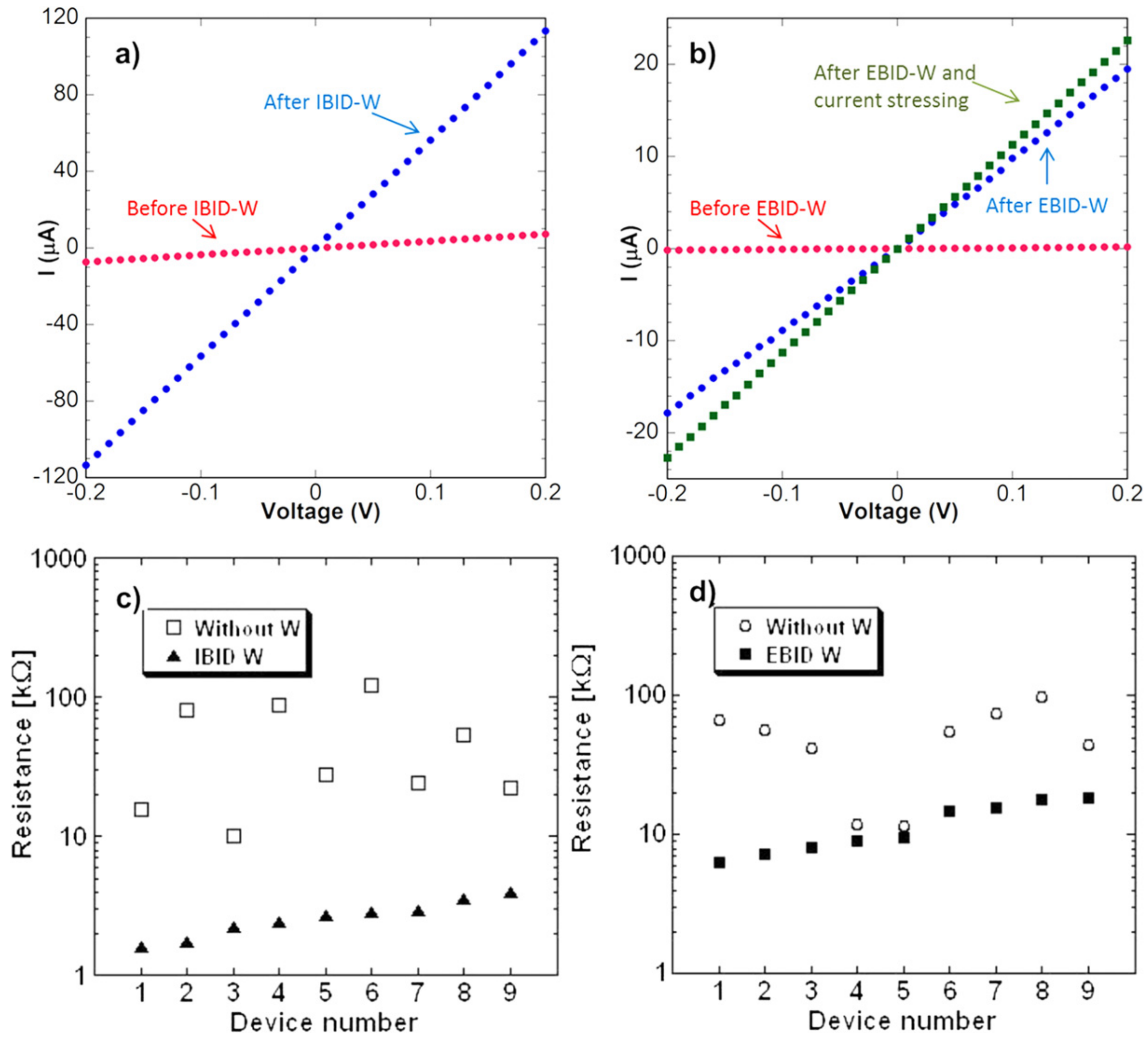

Figure 2. Typical *I–V* characteristics of CNF devices before and after (a) IBID-W and (b) EBID-W depositions. Resistances of CNF test devices with and without (c) IBID-W and (d) EBID-W contacts. Devices are numbered in increasing order of their final resistance values.

500 nm × 1000 nm for EBID-W and 1000 nm × 1000 nm for IBID-W. The composition of the deposited material is important since impurities in the deposits could lead to higher contact resistance. Figure 1(a) shows the SEM image of a typical CNF test device with an IBID-W contact. Figures 1(b) and (c) show a schematic of current paths at the contact and the corresponding equivalent circuit model, respectively, upon which the analysis of conduction across contacts presented in section 3 is based.

Figure 2 shows typical measured *I–V* characteristics for devices before and after IBID-W and EBID-W depositions, respectively, and the total resistances (obtained from *I–V*) of nine CNF test devices for each technique. Diameters of CNFs range from 100 nm to 215 nm, and the lengths of CNFs between W deposits vary between 1.8 μm and 10.6 μm. All test devices show reduction in resistance after W deposition. In all cases without W, the *I–V* curves are highly nonlinear as shown in figures 2(a) and (b), suggesting large contact resistance. After W deposition, the *I–V* behavior of each test device becomes linear and the total resistance decreases significantly. The resistances of CNFs with EBID-W (figure 2(d)) are larger than those with IBID-W (figure 2(c)) for all test devices.

Current stressing in vacuum is then applied to CNF test devices with W-deposited contacts to further reduce their resistances. The resistance versus stress current behaviors for four test devices each with IBID-W and EBID-W contacts, respectively, are shown in figures 3(a) and (b). Stress currents are applied up to 500 μA, in 100 μA intervals for 3 min in each stress cycle, with *I–V* characteristics measured after each stress cycle. This current stressing is expected to provide significant Joule heating to anneal the contacts [16, 28]. The resistance of EBID-W devices decreases with increasing stress currents, as revealed by the *I–V* measurements. However, the resistance of each device with IBID-W remains virtually unchanged throughout the stress cycles. This result indicates that while the IBID-W process produces stable electrode contacts with low resistance, the contact resistance of test devices with EBID-W needs further improvement by Joule heating to achieve similar resistance values. To confirm

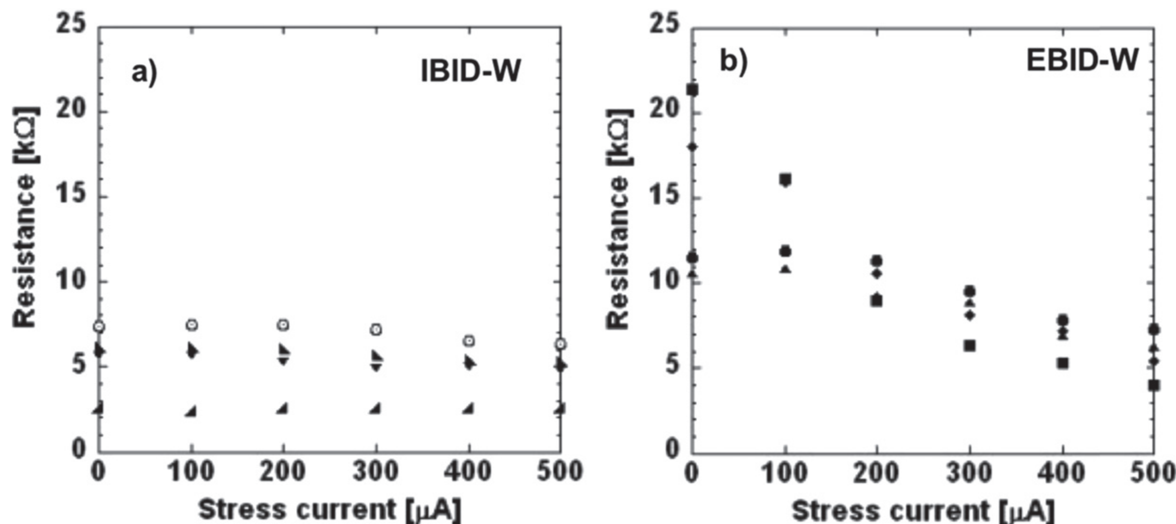

Figure 3. Resistances of CNF test devices with (a) IBID-W and (b) EBID-W contacts as a function of stress current in vacuum. Resistances are obtained from *I–V* measurements after each stress cycle. Four devices for each deposition are shown with each symbol corresponding to a different device.

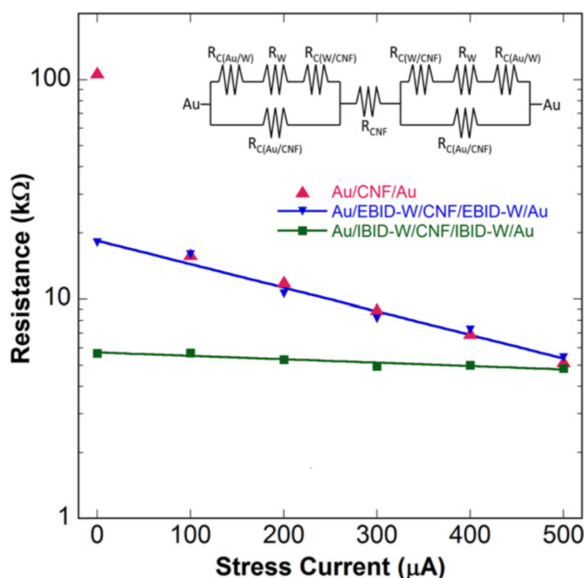

Figure 4. Comparison of resistances of three CNF test devices under current stressing in vacuum. Device without W is 150 nm in diameter, with length of 1.7 μm between electrodes. EBID-W device is 138 nm in diameter with length of 1.6 μm. IBID-W device is 150 nm in diameter with length of 2.0 μm.

this finding, an EBID-W and an IBID-W test device are both annealed in vacuum at 450 °C for 3.5 h, yielding similar improvements in resistance for the EBID-W device, whereas the resistance of an IBID-W test device remains unchanged after the same treatment.

3. Results and discussion

Figure 4 presents a comparison of results of resistance versus stress current behaviors for three CNF test devices with similar dimensions, all measured in vacuum. The as-drop-casted device shows a high initial resistance due to poor CNF/Au contacts, with conduction across them dominated by tunneling [28]. Upon moderate current stressing, localized Joule heating at the electrode interface reduces the contact resistance considerably.

This phenomenon is attributed to a reduction in the effective tunneling gap at the CNF/Au interface [28]. At stress currents above 100 μA, the Joule heat has the effect of flattening this interface, increasing the contact area and thus reducing the contact resistance further. Since the bonding between Au and C atoms on the CNF surface is weak and the solubility of carbon in Au is low [31, 32, 34], this resistance reduction is a manifestation of improvement in the wetting at the CNF/Au interface [28, 32]. Although the contact resistance between Au and CNF is known to be high [31], improved wetting brought upon by current stressing reduces the resistance by enhancing the effective contact area [35]. The results for the other two devices shown in figure 4, with IBID-W and EBID-W contacts, respectively, are similar to their counterparts in figure 3. They are shown here for the sole purpose of examining and correlating the conduction processes at the three different CNF/electrode contacts.

First, we identify the various conducting paths at a CNF/Au/W contact, as illustrated in figure 1(b). Each path is represented by a resistor in an equivalent circuit model for the entire contact, as shown in figure 1(c). The circuit model is reproduced as an inset in figure 4. The model consists of two parallel conduction paths, one through the CNF/Au interface ($R_{C(Au/CNF)}$), and the other is through a series combination of Au/W interface ($R_{C(Au/W)}$), W bulk (R_W), and CNF/W interface ($R_{C(W/CNF)}$). The resistances of the Au pad and the probe/Au contact are assumed to be negligible.

To assess the resistance components $R_{C(Au/W)}$ and R_W, a W line bridging two Au electrodes is fabricated using EBID, with its SEM image shown in figure 5. The total resistance of the W line, including the contacts with Au, amounts to about

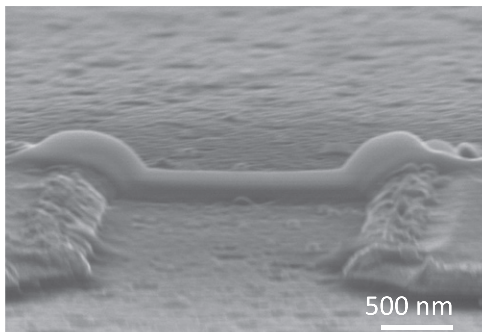

Figure 5. SEM image of a W line between Au electrodes. The W line formed by EBID is used to assess the resistance components $R_{C(Au/W)}$ and R_W in figure 1(c).

15 Ω after current stressing at 500 μA. This result indicates that the contributions of $R_{C(Au/W)}$ and R_W are insignificant as the total resistance of a CNF test device is in the kΩ range upon current stressing. Thus $R_{C(W/CNF)}$ is the only viable component of the series combination in the circuit model for the CNF/Au/W contact. Based on our knowledge of IBID and EBID, it is reasonable to expect similar findings had the W line been fabricated using IBID [9].

By comparing the resistance behavior of the CNF device with IBID-W contacts with that without W shown in figure 4, it is apparent that the $R_{C(Au/CNF)}$ component is sufficiently larger than $R_{C(W/CNF)}$ that it contributes little to the total contact resistance. Assuming that $R_{C(W/CNF)}$ is unaffected by current stressing due to the clean and abrupt as-deposited CNF/W interface (confirmed by interfacial nanostructural analysis presented in the following paragraphs), and knowing that the CNF resistance varies little with Joule heating until near breakdown [16, 22, 36], the total resistance must also be unaffected by current stressing, as demonstrated by the results in figure 3(a). On the other hand, the as-deposited CNF/EBID–W interface is less abrupt (again confirmed by interfacial nanostructural analysis) resulting in higher initial $R_{C(W/CNF)}$. Therefore, the contribution from $R_{C(Au/CNF)}$ throughout the current stressing cycles cannot be ignored and the total contact resistance becomes that from the parallel combination of $R_{C(Au/CNF)}$ and $R_{C(W/CNF)}$. At a stress current of 500 μA, both $R_{C(Au/CNF)}$ and $R_{C(W/CNF)}$ improve considerably and the total resistance of the EBID-W device approaches that of the IBID-W.

To examine the CNF/W interface and to correlate its nanostructure with the test device electrical behavior, we have obtained TEM cross-sectional images as shown in figure 6. The ultra-thin slices (or lamellas) of a W–CNF–Au electrode contact region as illustrated in the inset of figure 6(a) are prepared with FIB, allowing TEM imaging of 20 nm cross-sections of an IBID-W (figures 6(a) and (b)), EBID-W (figure 6(c)), and annealed EBID-W (figure 6(d)) contacts. For the IBID-W contact, the W deposit forms a clean and abrupt interface with CNF, as illustrated in figures 6(a) and (b), and appears to be a continuous polycrystalline layer. And the interfacial nanostructure does not change with current stressing. For such an interface, the contact resistance is much lower than that of CNF/Au so that the bulk of the carriers must flow through the Au–W–CNF path (see figures 1(b) and (c)) for all current stressing cycles. This is completely consistent with the observed behaviors of IBID-W devices shown in figures 3(a) and 4. In fact, the interface image suggests that the contacts in IBID-W devices are electrically optimal, so that there is little room for further improvement from current stressing. This is attributed to the high degree of crystallinity and purity in as-deposited IBID-W, which is confirmed by the high-resolution TEM image in figure 6(b). Further, the diffraction pattern from Fourier transform analysis of the interface suggests that the IBID-W deposit consists of large, randomly oriented crystallites with interplanar spacing of about 2.3 Å, compared to 2.2 Å for W (110). As indicated by the EDS results in the inset of figure 6(b), the IBID-W deposit has a significant amount of Ga, but contains negligible amounts of oxygen and carbon, thus ruling out significant oxide or carbide formations.

The EBID-W deposits shown in figures 6(c) and (d)) display a lighter contrast and a much less abrupt interface with CNF, with small W grains embedded in a carbon matrix. Unlike IBID-W devices, EBID-W ones yield a significant resistance decrease upon current stressing, as shown in figure 3(b). Since the CNF resistance is not affected by current stressing before approaching breakdown, this resistance reduction is most likely due to improvements in both CNF/Au and CNF/W interfaces. And such reduction is consistent with effective increases in both interface areas.

The decrease in contact resistance between EBID-W deposit and CNF might be partly due to a reduction of adsorbates such as water, oxygen and carbon at the CNF/W interface. As shown in the EDS spectrum for the as-deposited W (inset of figure 6(c)), the EBID-W device contains a considerable amount of carbon and oxygen. Since the precursor gas for EBID-W does not contain carbon, the origin of this carbon is due to residual impurities in the SEM chamber. These deposits resemble those reported elsewhere with similar conditions and precursor gas, which resulted in WO_3 and WC along with W nanocrystals [37]. However, the current-stressed EBID-W device contains larger W grains, as revealed in figure 6(d), and its inset displays an EDS spectrum showing negligible amounts of carbon and oxygen. Both observations are consistent with resistance reduction in the EBID-W devices due to current stressing [38].

High-current stressing was reported to be a viable purification method for W-wires fabricated with IBID [39], in which amorphous W was embedded in a carbon matrix. In that report, current stressing resulted in a significant decrease in the W resistivity, accompanied by an increase in the granularity of the deposited W [39]. In the W line reported earlier in this paper, the resistance decreases from 450 Ω to 15 Ω after current stressing at 500 μA. However, the outer surface of the W line remains highly resistive (>10^9 Ω) when probed directly. This finding, along with figure 6(c), indicates that the W deposit from EBID is generally not homogenous but a mixture of elemental W and compounds, some of which are probably non-conductive. The EDS results in figures 6(c) and (d) show that the EBID-W deposit contains significant amounts of oxygen and carbon, which are reduced drastically by current stressing.

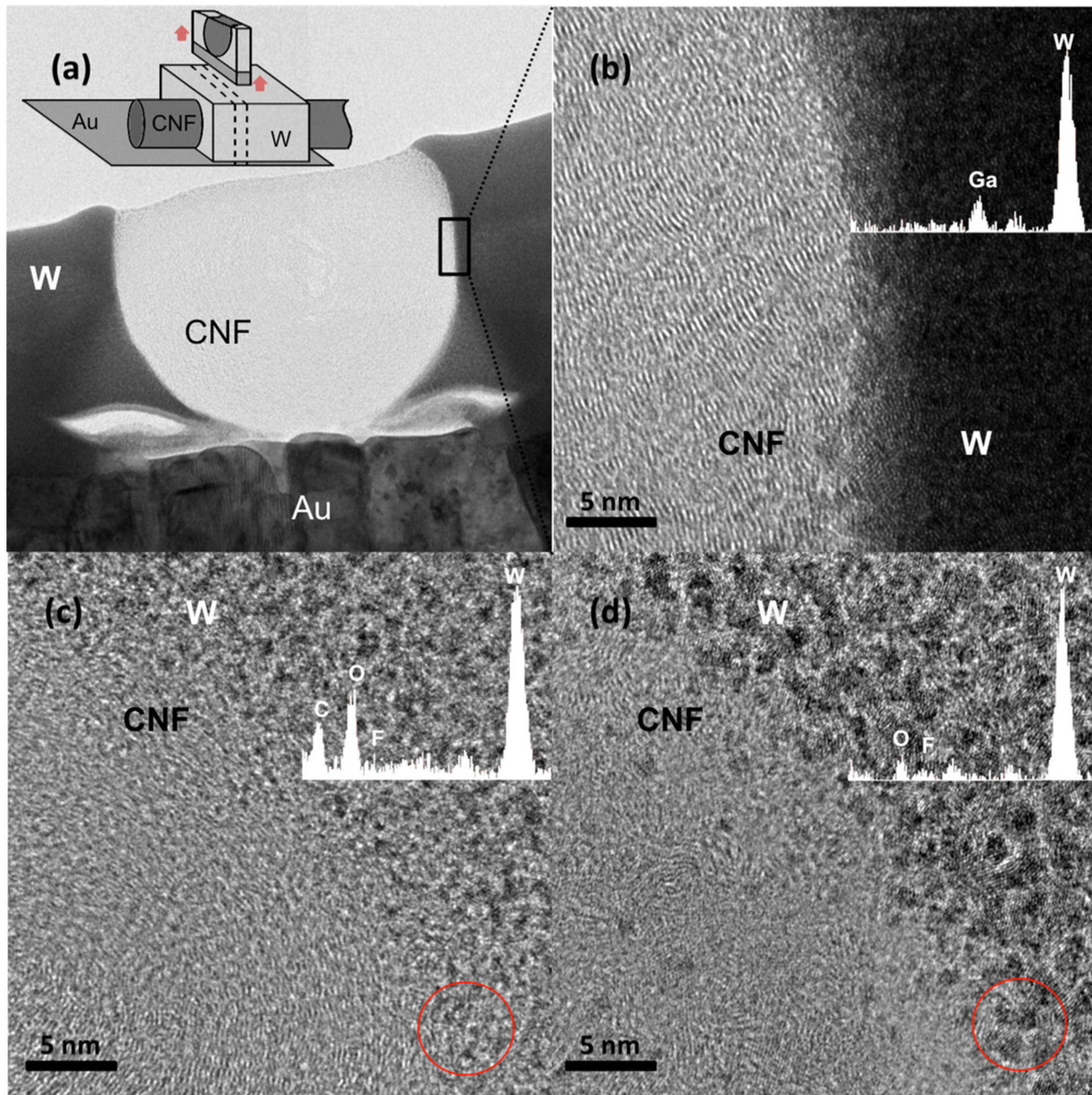

Figure 6. (a) Bright-field TEM cross-sectional view of the CNF–Au–W electrode contact (IBID), with an inset containing a schematic of the contact region and the ultra-thin slice from which the image was obtained. Voids at the intersection of all three materials are present as a result of the CNFs' shadow during W deposition. (b) High-resolution image of the IBID-W contact shows a clean interface with CNF, with the inset displaying EDS results for W deposit near the interface. (c), (d) Circled region exemplifies difference in W grain sizes before (c) and after anneal (d). (c) Before current stressing, EBID-W contact reveals small W grains (darker spots) embedded in a carbon matrix. The interface is less abrupt than that in (b) due to the similar contrasts of C within the CNF and W deposit. (d) W grain size in EBID-W contact increases after current stressing. Contrast at the interface is increased due to larger W grains and C reduction. Insets in (c) and (d) display EDS results for W deposits near their respective interfaces, showing W/O atomic ratio increases from 0.37 to 1.4 (weight ratio from 4.3 to 16) due to current stressing. Carbon content is considerably reduced by current stressing to a negligible amount, from an initial W/C atomic ratio of 0.33.

Stress current can generate oxygen and carbon vacancies, which may result in the formation of conduction filaments [40], in addition to other changes in the deposit. This finding suggests that oxygen and carbon content reduction can also be responsible for contact resistance improvement, in addition to the increase in W grain size. Purification of the W deposits, along with enhanced crystallinity, can lead to higher W conductivity and lower contact resistance.

It is clear from the TEM images that EBID-W and IBID-W produce significantly different W deposits and CNF/W interfaces. This is partly due to the relatively high base pressure for the EBID-W technique, compared with IBID-W, and different source gases. In addition, IBID has a higher impinging energy during deposition, which may result in localized heating around the deposition area as well as sputtering of adsorbates from the surface, resulting in purer deposits than those from EBID [9]. Despite these differences, our results show that both W deposition schemes are effective in reducing the overall resistance of the CNF test devices.

Extracting accurate values of contact resistance is challenging in part because the W deposits are usually recessed from the electrode edge (figure 1(a)), making CNF length estimations difficult. However, upper limits for the values of the contact resistance can be established by considering the length of the CNF to be the portion measured from the edges of the electrodes. This estimation results in the lower limit for CNF resistance and the upper limit for contact resistance. Based on this assumption and four-point measurements, we obtain an average CNF resistivity of $1.1 \times 10^{-3}\ \Omega\,\mathrm{cm}$ among the devices consisting of CNFs from the same growth, consistent with results reported previously [28, 41]. The corresponding contact resistances are 2.0–3.5 kΩ for IBID-W devices, and 2.8–5.8 kΩ for EBID-W devices. Thus for CNF devices with either IBID-W or EBID-W contact, the contact resistance is a significant component of the total resistance. For comparison, contact resistance between CNTs and Ti/Au electrodes, deposited by thermal evaporation, ranged from 1.56 kΩ to 3.28 kΩ [42]. In this case, the CNT contact is encapsulated by a thin layer of Ti, which is known to yield lower contact resistance than Au or W [31, 43], followed by a thicker Au deposit. More recently, extremely low MWNT device resistance ($116 \pm 0.1\ \Omega$) obtained using EBID of amorphous carbon subsequently graphitized by annealing the contact was reported [44]. In this case, the carbon deposits were performed on the edges of the CNT/electrode contact in order to connect multiple shells directly to the EBID contact.

4. Conclusion

As contact resistance remains a dominant issue in on-chip interconnects, W deposition using EBID and IBID is shown to reduce CNF interconnect test device resistance significantly. IBID-W is generally more effective in reducing the contact resistance, but EBID-W produces similar contact resistance reductions, which can be further improved by current stressing to yield values comparable to that for IBID-W. And analysis of the conduction process at each contact correlates well with observed interfacial nanostructures. However, challenges remain for either contact engineering technique. Despite the higher purity of the IBID-W deposit, it contains a significant amount of Ga, which is undesirable for IC applications. In order to obtain comparable improvements using EBID-W, current stressing is necessary but Joule heat generated in the process can be undesirable for other devices on the same chip. Purer deposits may be possible for EBID-W, but it is unlikely that the grain size would increase and oxygen content would decrease without further current stressing [39, 41].

Acknowledgments

We are grateful for the technical assistance from Atsushi Muto, Larry Cessna, and Jamil Clarke of Hitachi High Technologies America in the IBID-W experiments.

References

[1] Choi Y R, Rack P D, Frost B and Joy D C 2007 *Scanning* **29** 171–6

[2] Rack P D, Fowlkes J D and Randolph S J 2007 *Nanotechnology* **18** 465601

[3] Randolph S J, Fowlkes J D and Rack P D 2006 *Crit. Rev. Solid State Mater. Sci.* **31** 55

[4] Brintlinger T, Fuhrer M S, Melngailis J, Utke I, Bret T, Perentes A, Hoffmann P, Abourida M and Doppelt P 2005 *J. Vac. Sci. Technol.* B **23** 3174

[5] Molhave K, Madsen D N, Dohn S and Boggild P 2004 *Nanotechnology* **15** 1047

[6] Utke I, Hoffmann P and Melngailis J 2008 *J. Vac. Sci. Technol.* B **26** 1197

[7] Koops H W P, Schossler C, Kaya A and Weber M 1996 *J. Vac. Sci. Technol.* B **14** 4105

[8] Lau Y M, Chee P C, Thong J T L and Ng V 2002 *J. Vac. Sci. Technol.* A **20** 1295

[9] Botman A, Mulders J J L and Hagen C W 2009 *Nanotechnology* **20** 372001

[10] Rubanov S and Munroe P R 2004 *J. Microsc.* **214** 213

[11] Shedd G M, Lezec H, Dubner A D and Melngailis J 1986 *Appl. Phys. Lett.* **49** 1584

[12] Tao T, Ro J, Melngailis J, Xue Z and Kaesz H D 1990 *J. Vac. Sci. Technol.* B **8** 1826

[13] Castillo R C 2014 *Functional Nanostructures Fabricated by Focused Electron/Ion Beam Induced Deposition* (Berlin: Spinger)

[14] Brunel D, Troadec D, Hourlier D, Deresmes D, Zdrojek M and Melin T 2011 *Microelectron. Eng.* **88** 1569

[15] Wei B Q, Vajtai R and Ajayan P M 2001 *Appl. Phys. Lett.* **79** 1172

[16] Saito T, Yamada T, Fabris D, Kitsuki H, Wilhite P, Suzuki M and Yang C Y 2008 *Appl. Phys. Lett.* **93** 102108

[17] Kreupl F, Graham A P, Duesberg G S, Steinhogl W, Liebau M, Unger E and Honlein W 2002 *Microelectron. Eng.* **64** 399

[18] Li J, Ye Q, Cassell A M, Ng H T, Stevens R, Han J and Meyyappan M 2003 *Appl. Phys. Lett.* **82** 2491

[19] Nihei M, Kawabata A, Kondo D, Horibe M, Sato S and Awano Y 2005 *Japan. J. Appl. Phys., Part 1* **44** 1626

[20] Zhang L, Austin D, Merkulov V I, Meleshko A V, Klein K L, Guillorn M A, Lowndes D H and Simpson M L 2004 *Appl. Phys. Lett.* **84** 3972

[21] Melechko A V, Merkulov V I, McKnight T E, Guillorn M A, Klein K L, Lowndes D H and Simpson M L 2005 *J. Appl. Phys.* **97** 041301

[22] Ngo Q, Yamada T, Suzuki M, Ominami Y, Cassell A M, Li J, Meyyappan M and Yang C Y 2007 *IEEE Trans. Nanotechnol.* **6** 688

[23] Naeemi A and Meindl J D 2009 *Annu. Rev. Mater. Res.* **39** 255–75

[24] Pop E, Mann D, Cao J, Wang Q, Goodson K and Dai H 2005 *Phys. Rev. Lett.* **95** 155505

[25] Li H, Xu C and Banerjee K 2010 *IEEE Des. Test Comput.* **27** 20

[26] De Volder M F L, Tawfick S H, Baughman R H and Hart A J 2013 *Science* **339** 535–9

[27] 2011 International Technology Roadmap for Semiconductors, with 2012 updates, available online at www.itrs.net/Links/2012ITRS/Home2012.htm

[28] Yamada T, Saito T, Suzuki M, Wilhite P, Sun X, Akhavantafti N, Fabris D and Yang C Y 2010 *J. Appl. Phys.* **107** 044304
Yamada T 2001 *Appl. Phys. Lett.* **78** 1739

[29] Li K, Wu R, Wilhite P, Khera V, Krishnan S, Sun X and Yang C Y 2010 *Appl. Phys. Lett.* **97** 253109

[30] Wu W, Krishnan S, Yamada T, Sun X H, Wilhite P, Wu R, Li K and Yang C Y 2009 *Appl. Phys. Lett.* **94** 163113
[31] Matsuda Y, Deng W Q and Goddard W A 2007 *J. Phys. Chem.* C **111** 11113
[32] Lim S C, Jang J H, Bae D J, Han G H, Lee S, Yeo I S and Lee Y H 2009 *Appl. Phys. Lett.* **95** 264103
[33] Joy D C and Rack P D 2005 *Microsc. Microanal.* **11** 816
[34] Maiti A and Ricca A 2004 *Chem. Phys. Lett.* **395** 7
[35] Asaka K, Karita M and Saito Y 2011 *Appl. Surf. Sci.* **257** 2850
[36] Suzuki M, Ominami Y, Ngo Q, Cassell A M, Li J and Yang C Y 2007 *J. Appl. Phys.* **101** 1143071–5
[37] Li J, Toth M, Tileli V, Dunn K A, Lobo C J and Thiel B L 2008 *App. Phys. Lett.* **93** 023130
[38] Park H L, Park C D and Chun J S 1988 *Thin Solid Films* **166** 37
[39] Prestigiacomo M, Bedu F, Jandard F, Tonneau D, Dallaporta H, Roussel L and Sudraud P 2005 *Appl. Phys. Lett.* **86** 192112
[40] Wong H-S P, Chen Y-S, Wu Y, Chen P-S, Lee B, Chen F T and Tsai M-J 2012 *Proc. IEEE* **100** 1951
[41] Reuger A, Bedu F, Tonneau D, Dallaporta H, Prestigiacomo M, Houel A and Sudraud P 2008 *J. Vac. Sci. Technol.* B **26** 1175
[42] Lan C, Srisungsitthisunti P, Amama P B, Fisher T S, Xu X and Reifenberger R G 2008 *Nanotechnology* **19** 125703
[43] Lim S C, Jang J H, Bae D J, Han G H, Lee S, Yeo I S and Lee Y H 2009 *Appl. Phys. Lett.* **95** 264103
[44] Kim S, Kulkarni D D, Rykaczewski K, Henry M, Tsukruk V V and Federov A G 2012 *IEEE Trans. Nanotechnol.* **11** 1223